Chemistry and Materials Research
ISSN 2224- 3224 (Print) ISSN 2225- 0956 (Online)
Vol.8 No.6, 2016

Preparation and Characterization of Various Interstitial N-Doped TiO_2 Catalysts from Different Nitrogen Dopants for the Treatment of Polluted Water

M. A. Shehata[*1] Sayed A. Shama[1] Sawsan A. Mahmoud[2] M. M. Doheim[2]
1.Faculty of Science, Benha University, Fred Nada Street, Benha, Egypt
2.Development of processes Department, Egyptian Petroleum Research Institute (EPRI), 1Ahmed El-Zomer, Nasr City, Box. No. 11727, Cairo, Egypt

Abstract
In this work N-doped TiO_2 nano particle photocatalysts were prepared through a sol-gel procedure using three different types of nitrogen dopants urea, diethanolamine (DEA) and triethylamine (TEN). Multiple techniques (XRD, TEM, SEM, EDX, BET, Raman and UV-Visible absorption) were commanded to characterize the crystal structure of N-doped TiO_2. The catalytic activity of the N-doped TiO_2 under ultraviolet (UV) and visible light irradiation is evidenced by the decomposition of 2-chlorophenol, showing that nitrogen atoms in the N-doped TiO_2 are responsible for the visible light catalytic activity. It is suggested that doped nitrogen here is located at the interstitial site of TiO_2 lattice. Amongst investigated nitrogen precursors diethanolamine provided the highest visible light absorption ability of interstitial N-doped TiO2 with the smallest energy band gap and the smallest anatase crystal size, resulting in the highest efficiency in 2-cholorophenol degradation. The photocatalytic activity and 2-CP mineralization ability of all N-doped TiO_2 can be arranged in the following order: TiO_2/DEA > TiO_2/TEN > TiO_2/UREA > un-doped TiO_2.
Keywords: 2-chlorophenol, Photocatalytic degradation, N-doped TiO_2, Different Nitrogen Dopants, urea, diethanolamine (DEA), triethylamine (TEN) and Catalytic Activity.

1. Introduction

Since the report of photo electrochemical decomposition of water on titanium dioxide electrode in 1972 [1], the chemical stability, non toxicity, and high photocatalytic reactivity of TiO_2 has attracted tremendous attention. However, TiO_2 without doping is active only by irradiating with ultraviolet light because of its large band gap of 3.2 Ev (anatase). This band gap limits the use of the wide energy window of sun light because solar energy is the most important alternative energy source in the future [2]. Among these studies, nitrogen doping [3-6] is one of the most important methods for a promising application.

In industry and daily life, phenolic compounds are widely used and have become common pollutants in water bodies. Eleven phenolic compounds have been listed by USEPA as priority pollutants [7]. Due to their stability and bio-accumulation, they remain in the environment for longer periods. As they have high toxicity and a carcinogenic character, they have caused considerable damage and threat to the ecosystem in water bodies and human health. An effective and economic treatment for eliminating phenolics in water has been in urgent demand. Traditional wastewater treatment techniques include activated carbon adsorption [8], chemical oxidation, biological digestion, etc. However, in each technique there are limitations and disadvantages. For instance, activated carbon adsorption only involves phase transfer of pollutants without decomposition, but this induces another pollution problem [9]. Chemical oxidation is unable to mineralize all organic substances and is only economically suitable for the removal of pollutants in high concentrations [10-12]. For biological treatment, the slow reaction rates, disposal of activated sludges and control of proper pH and temperature are the drawbacks to be considered [13, 14]. The current trend in treatment has moved from phase transfer to destruction of pollutants such as advanced oxidation process (AOP). This involves reactive free radical species for non-selective mineralization of organic compounds to harmless end products [15]. The use of titanium dioxide as a semiconductor catalyst under UV-light belongs to AOP with potential in wastewater treatment. Photocatalytic process has the following advantages [16]: Complete oxidation of organic pollutants in a few hours, without production of polycyclic products, highly active catalyst adaptable to specially designed reactor system and Oxidation of pollutant in ppb range.

2. Experimental

2.1. *Catalyst preparation*

A modified sol-gel method was used to synthesis N-doped TiO2 with a mole ratio of 1:20:1:1:1 for TTiP: EtOH: HNO3:H2O: dopant (DEA, TEN,UREA). First TTiP was dissolved in EtOH, and the solution was stirred for 30 min. in a second solution, EtOH was mixed with H2O that contained HNO3. This solution was stirred to promote hydrolysis until transparent. After mixing both portions, precipitation readily occurred. The dopant was then added to the solution.

For comparison, TiO2 without a dopant was prepared using the same method (Labeled as un-doped TiO2).

The homogeneous transparent solution was then kept under stirring conditions for 30 minute at 4 oC before undergoing the drying process. After drying at 100 oC for 90 min, the powder was collected and calcined at 400 oC in an electric tube furnace in a N2 atmosphere. The samples were held at the peak temperature for 30 min and then cooled to room temperature. A commercial grade Degussa P-25 TiO2 was used as a reference.

2.2. *Catalyst characterization*

XRD analysis was performed using a PAN analytical X'Pert PRO diffractometer in reflection mode using CuKα radiation (λ = 0.1542 nm) at 40 Kv and 40 mA,over the scan range of 2θ between 20 and 80 at 295 K, in order to identify the phase present.

Transmission Electron Microscopy (TEM) studies were carried out using a JEOL JEM-2100 electron microscope operating at 120 kV. BET surface area of the synthesized samples were measured on Quantachrome NOVA 2000 system (USA), at −196 °C after degassing at 300 °C and 10−5 mmHg for 4 h. Scanning Electron Microscopy (SEM) investigation was performed by JEOL JEM 3500 electron microscope to confirm the surface morphology of the prepared materials. Energy Dispersive X-ray Spectroscopy (EDX) is a chemical microanalysis technique used in conjunction with SEM to characterize the elemental composition of the prepared material. UV-Vis absorption spectrum was measured at room temperature in the range from 200 to 2500 nm using a Scan UV-Vis spectrophotometer (type JASCO corp., V-570, Rel-00, Japan). Raman spectroscopy is carried out using Bruker SENTERRA dispersive Raman microscope (λ = 532 nm).

2.3. *Photocatalytic activity measurement*

Quartz batch photoreactor of cylindrical shape ,containing 500 ml of aqueous suspension, was used for performing the reactivity experiments. A magnetic stirrer guaranteed a satisfactory suspension of the photocatalyst and the uniformity of the reacting mixture. UV-vis lamp (365 nm) was axially immersed within the photoreactor and it was cooled by water circulating through a quartz thimble; the temperature of the suspension was about 300 K. The initial concentration of 2-CP was 100 ppm. The polluted water was aerated using a bubble distributor. The experiments were performed at room temperature and the pH of the reaction mixture was kept at 5.5. Prior irradiation, the slurry was aerated for 10 min at dark to reach adsorption equilibrium followed by UV-vis irradiation. Adequate aliquots (5 cm3) of the sample were withdrawn after periodic interval of irradiation and analyzed after filtration using: (a) HPLC PerkinElmer series 200 provided with photodiode array detector at 280 nm wavelength and C8 column (4.6 cm×25 cm). The mobile phase was acetonitrile/water in the ratio of 60:40 (v/v) with a flow rate of 1 ml/min. (b) Ion chromatograph (Dionex-pac) was used to determine the concentration of chloride and acetate ions.

3. Results and Discussion

3.1. *XRD*

As shown in the x-ray diffraction patterns Figure (1) , it can be seen that, in general, all the powder are well crystalline materials, commercial Degussa P-25 catalysts consist of about 25 % rutile phase and 75 % anatase according to (ICDD card NO. 04-008-7849) and non-doped TiO2 catalysts consist of about 5 % rutile phase and 95 % anatase . The anatase phase was predominant structure in N-doped TiO2 under all synthesis conditions. A major peak corresponding to (101) reflections of the anatase phase of TiO2 was apparent at the angle of 25.28 whilst the minor peaks appeared at 36.15, 41.33, 54.44, 62.89 and 69.17. The X-ray diffraction analysis of all samples revealed that only TiO2 obtained from DEA dopant had typical peaks of TiO2 anatase without any detectable peaks of rutile

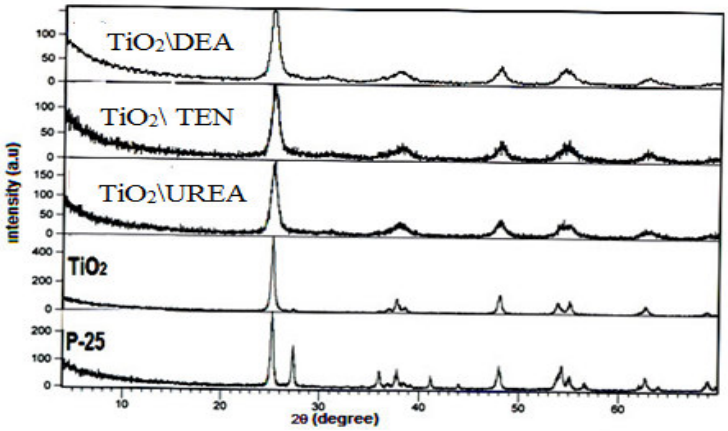

Figure 1. cumulative XRD diffractograms of commercial Degussa p-25, non-doped TiO2, and N-doped TiO2.

Weight fractions of each phase were calculated by the following equation:

WR = AR\0.884AA + AR

Where AA represents the integrated intensity of the anatase (101) peak and AR the integrated intensity of the rutile (110).

The crystal size was calculated using the scherrer equation [17] after correction for instrumental broadening.

$$d = \frac{B\lambda}{\beta \cos\theta}$$

While:

d = is the mean particle diameter.

B = is the Scherer constant (0.89).

λ = is the wave length of the X- ray beam (1.5405Å).

β = is the full width half maximum of the 101 anatase diffraction line.

Θ =is the diffraction line of the investigated phase.

The results are listed in Table (1). It can be seen that the doping of nitrogen decreases the grain size of TiO_2 significantly. There are three different main opinions regarding modification mechanism of TiO_2 doped with nitrogen.

Band gap narrowing: asashi et al. [18] found N2p state hybrids with O2p state in anatase TiO_2 doped with nitrogen because their energies are very close, and thus the band gap of N-TiO_2 is narrowed and able to absorb visible light.

Impurity energy level: irie, et al [19] stated that TiO_2 oxygen sites substituted by nitrogen atom form isolated impurity energy level above the valence band.

Irradiation with UV light excites electrons in both the valence band and the impurity energy level, but illumination with visible light only excites electrons in the impurity energy level.

Oxygen vacancies: Ihara, et al. [20] Concluded that oxygen-deficient sites formed in the grain boundaries are important to emerge vis-activity and nitrogen doped in part of oxygen-deficient sites are important as a blocker for reoxidation.

The modification mechanism of anatase doped with nitrogen was also analyzed by zhao et al. [21] They investigated N-TiO_2 and concluded that TiO_2 doped with substitutional nitrogen has shallow acceptor states above the valence state. In contrast, TiO_2 doped with intersititial nitrogen has isolated impurity states in the middle of the band gap. These impurity energy levels are mainly hybridized by N2p states and O2p states.

From Table (1) we can show the effect of N-doped on the crystallite size of the preparing solids. The crystallite size of all the samples is observed in the range from 39 to 11.3 nm. It is seen that the average crystallite size of doped Titania is smaller to that of un doped titania. The small particle size of N-doped TiO_2 increases the probability for reactions of the photo-generated electrons and holes with reactant molecules and hence enhances the photocatalytic activity.

Table 1. Effect of N- doped TiO_2 on the crystallite size of the preparing solids

Catalyst	crystallite size(nm)
P-25	39
Non-doped (TiO_2)	31
TiO_2\UREA	16
TiO_2\TEN	14
TiO_2\DEA	11.3

3.2. *UV–Visible absorption measurements*

UV–Visible spectra of the representative commercial Degussa P25, non-doped TiO_2, TiO_2\UREA, TiO_2\TEN and TiO_2\DEA samples are shown in Figure (2). The wave length is 384,395,426,435 and 480 for pure TiO_2, P-25, TiO_2\UREA, TiO_2\TEN and TiO_2\DEA respectively. It can be seen that the absorption edge is found to shift in a systematic manner to longer wavelength with increasing content of nitrogen doping in Titania. This red shift was attributed to the charge-transfer transition between the d–electrons of the dopant and the conduction band of TiO_2 [22].

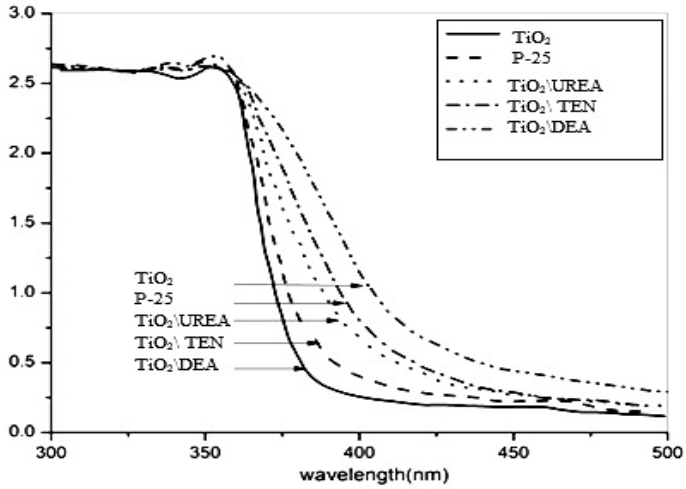

Figure 2. UV-visible spectra of commercial Degussa p-25, non-doped TiO_2, and N-doped TiO_2

From these spectra, the band gap energy (Eg) value of the samples was calculated using equation [23]:

$$\alpha h\nu = A\,(h\nu - Eg)n/2$$

Where α is the absorption coefficient, hν is the photon energy, n ~ 1 for direct transition between bands and Eg is the energy of the band gap. The simplification of the above equation into the formula:

$$Eg = 1240.82/\lambda$$

Where λ is the absorption band edge wavelength (nm).

For practical purposes, the energy band gap value was calculated by extrapolation of the absorption band to the x–axis. The band gap value of the samples is reported in Table (2).

Table (2) Band gap value of P-25, non-doped $TiO_2$and N-doped catalyst

Catalyst	Band gap (eV)
Non-doped (TiO2)	3.43
P-25	3.34
TiO2\UREA	3.11
TiO2\TEN	3.05
TiO2\DEA	2.84

This data clearly reveals that the band gap energy of doped TiO_2 samples decrease with increasing nitrogen composition in Titania host lattice. This is in good agreement with the previous reports. [17] With doping of nitrogen in the TiO_2 lattice, the band gap is lowered to 3.11, 3.05 and 2.84 eV for TiO_2\UREA, TiO_2\TEN and TiO_2\DEA respectively. This absorption enhancement with decrease in band gap in the visible region can be assigned to the formation of dopant level nearer the valance band; which results the excitation of N2+ 3d–electrons to the TiO_2 conduction band (charge transfer transition). The optical absorption measurement of doped samples is also manifested by change of the color of doped powders from light to dark yellow. This effect may be due to creation of trapping sites by doping of the nitrogen in the TiO_2 lattice, hence enabling the separation of photo–excited hole and electron pair, thus increasing the photocatalytic activity of the catalysts in the visible region.

3.3. *Raman spectroscopy*

The Raman shifts of N-doped TiO_2, non doped TiO_2 and P-25 TiO_2 were performed on a renishaw Raman imaging microscope operated with green laser. Si plate was used to calibrate Raman, which exhibited the evident Raman shift at 520 cm^{-1}. Each of the finely-ground samples was deposited on a glass and a little acetone solution was dropped in order to make the sample tightly attach each other and be easy to smooth its surface with a spatula.

Figure (3) shows the Raman spectra of different samples. Raman peak at about 146 cm^{-1} is the strongest of all the observed bands, which observed for all the samples, which is attributed to the main Eg anatase vibration mode. Moreover, vibration peaks at 199 cm^{-1} (Eg, weak), 399 cm^{-1} (B1g), 516 cm^{-1} (A1g) and 640 cm^{-1} (Eg) are presented in the spectra for all samples, which indicates that anatase TiO_2 crystalline are the predominant species [24]. Rutile phase have Raman peak at about 445 cm^{-1}(Eg) and 608 cm-1(A1g) observed in commercial Degussa P-25 and also 608 cm^{-1} (A1g) observed in non-doped TiO_2[25].

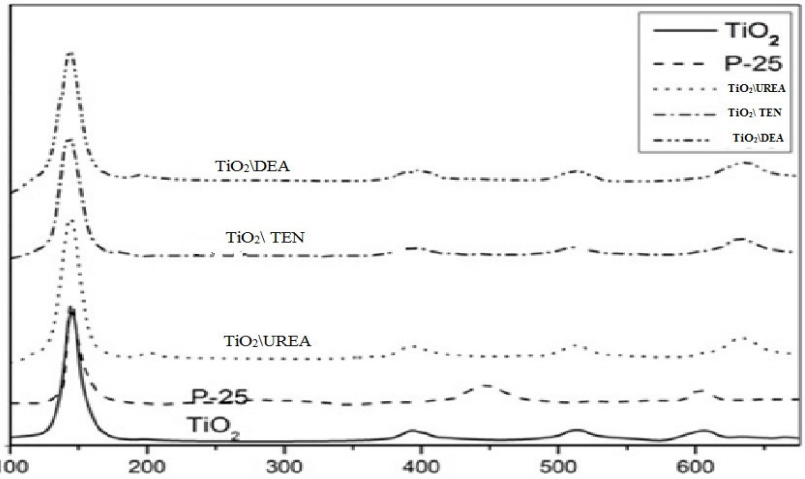

Figure 3. Raman spectra of commercial Degussa p-25, non-doped TiO_2, and N-doped TiO_2

3.4. *SEM*

Figure (4) shows The SEM micrographs of commercial Degussa P-25, non-doped TiO_2, TiO_2 \UREA, TiO_2 \DEA and TiO_2 \TEN samples. It can be seen that the morphology of the Degussa P-25 and non-doped TiO_2 powder is completely different from those of N-doped TiO_2 powders. In general, three types of investigated N-doped TiO_2 powders consist of nano-sized primary particles with spherical shape in agglomerated powder particles, whereas, P-25 and non-doped TiO_2 powder consists of relatively larger size of powder particles, where doped titania are smaller. There is no change in the morphology of three types of investigated N-doped TiO_2 after adding nitrogen ions that might be attributed to the nitrogen oxides are well dispersed within the TiO_2 phase.

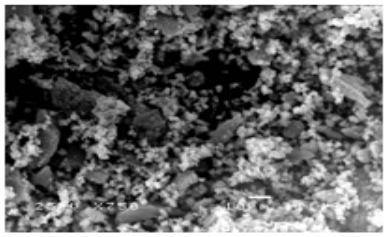

Degussa P-25

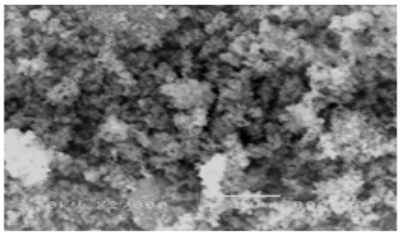

Non-doped TiO_2

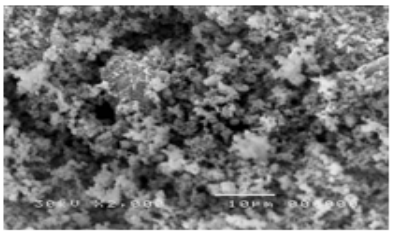

TiO_2 \UREA

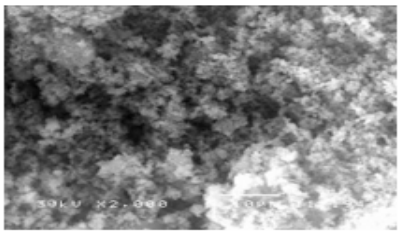

TiO_2 \TEN

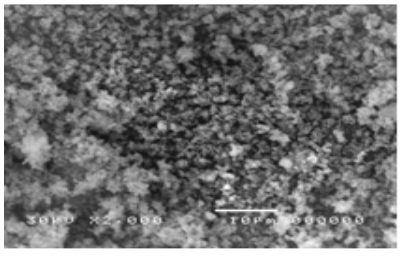

TiO_2 \DEA

Figure 4. SEM Micrographs of the non doped $TiO_2$and N-doped TiO_2samples

3.5. *TEM*

Figure (5) shows the transmission electron micrographs of commercial Degussa P-25, non-doped TiO_2,

TiO_2\UREA, TiO_2\TEN and TiO_2\DEA samples, It can be seen that the size of non-doped TiO_2 particles ranged from 39 to 31 nm. However, the size of doped particles with high concentration nitrogen ranged from 16 to 11.3 nm. It is evident from this micrograph that the nanoparticles become smaller and smaller as the doped nitrogen content increases, which is in close agreement with average crystallite size obtained from XRD studies. This is easy to be understood because doping foreign ions in TiO_2 lattice can actually prohibit the crystal growth. TEM investigations gave evidence of no segregated secondary phases of nitro oxides and supports homogeneously substitution in the TiO_2 matrix which is consistent with the results of XRD patterns and SEM micrographs.

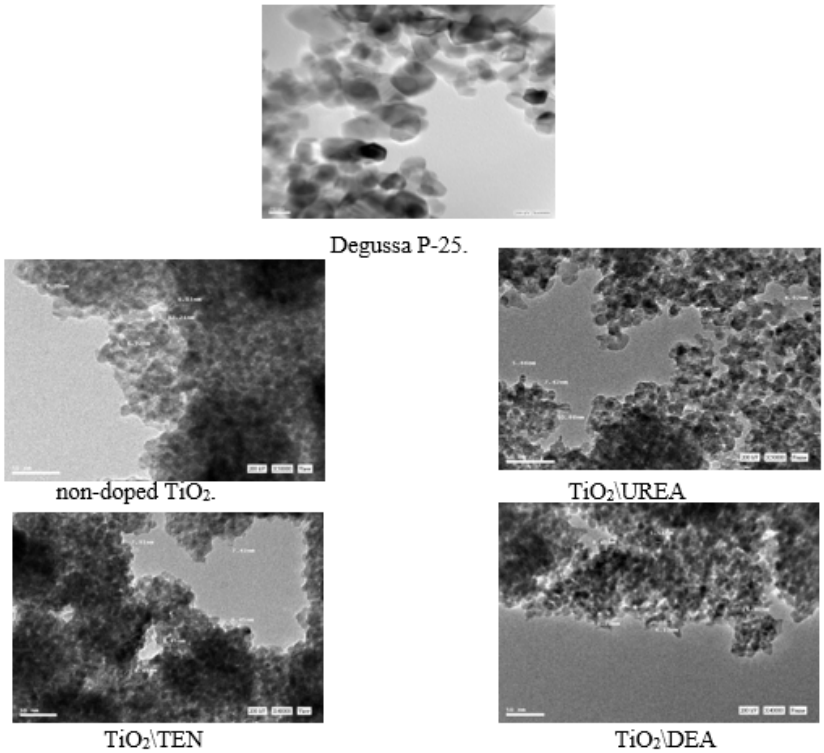

Figure 5. TEM Micrographs of the non doped $TiO_2$and N-doped TiO_2samples

3.6. *Energy Dispersive X-ray Spectroscopy (EDX)*

Figure (6) Shows nitrogen content in the (TiO_2\UREA, TiO_2\TEN and TiO_2\DEA) measured by EDX. In order to establish the achievement of the targeted chemical composition in the synthesized powders, the N-doped TiO_2 powder was examined by EDX analysis as depicted in Table (3) the chemical composition observed in EDX analysis confirms that the targeted chemical composition was achieved in the powders formed in sol-gel method. This information suggests that the chemical composition (N content) of N-doped TiO_2 largely depends on the molecular structure of the nitrogen dopant and the accessibility of nitrogen atoms to react with the Titania precursor

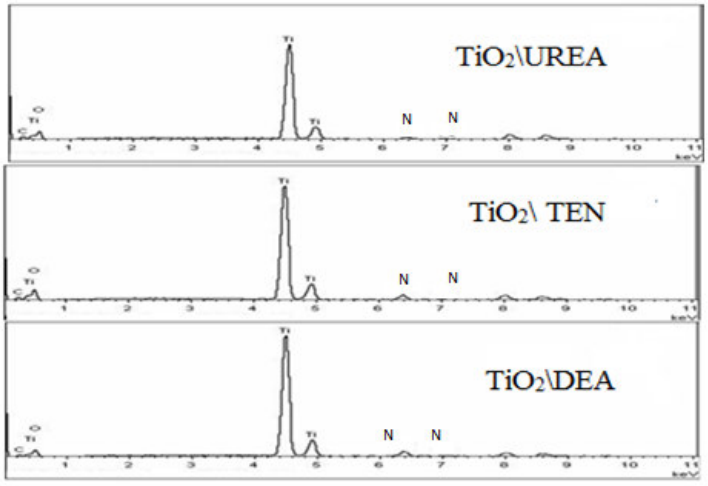

Figure 6. Nitrogen content in the N-doped TiO_2

Table (3) nitrogen content in the N- doped TiO_2 measured by EDX

Catalyst	wt. %
TiO_2\UREA	1.88
TiO_2\TEN	2.48
TiO_2\DEA	3.18

3.7. *Surface area measurement*

The BET surface was examined using N_2adsorption at the liquid nitrogen temperature in a constant volume adsorption apparatus. Before analyzing the sample, the surface area range must be controlled because the surface area calculation depends on a different math model. Different math models have different optimal condition. The values of surface area, Total pore volume and average pore size of the commercial Degussa P-25, non-doped TiO_2, TiO_2\UREA, TiO_2\TEN; and TiO_2\DEA catalysts determined by the BET method are shown in table 3.4. The surface area of non-doped TiO2 was diminished after doping the sample with nitrogen. When dopant concentration was further increased gradually, both crystallite size and BET surface area values are gradually decreased.

Table 4. Surface area of various solid powders.

Catalyst	BET (m2/g)	Total pore volume (cc/g)	Average pore size (nm)
P- 25	288.1	0.018	22.76
TiO_2	216	0.090	11.37
TiO_2\UREA	57.78	0.026	21.90
TiO_2\TEN	54.52	0.023	21.64
TiO_2\DEA	44.96	0.020	21.95

3.8. *Photocatalytic activities of photocatalysts*

In the present study, the samples that were doped at various ratios of nitrogen to Titania were tested by the photo degradation of 2-chlorophenol (2-CP). Figure.7. shows the effect of the reaction time on the photo degradation of 2-chlorophenol from the polluted water. After 180 min of testing, the percentage degradation was 50, 53, 44, 57and 65 wt% for bare TiO_2, P-25, TiO_2\UREA, TiO_2\TEN and TiO_2\DEA respectively. It can be seen that the more nitrogen ion that was doped, the greater increase in the rate of degradation of 2-CP. As the concentration of nitrogen increased in TiO_2, the photocatalytic efficiency was gradually increased. TiO_2\DEA powder showed the highest photocatalytic activity. This increase in photocatalytic activity with nitrogen doping is related to shift in optical absorption of the catalyst in visible region. TiO_2 absorbs only UV energy (below 400nm) whereas N- doped TiO_2 catalyst absorbs UV and portion of visible energy hence there is increase in photo-catalytic activity. It was apparent that nitrogen doping has an effect on hindrance of anatase crystal growth; therefore the crystallite sizes of TiO_2\DEA nanoparticles (11.3 nm) are smaller than those of pure TiO_2 (31 nm), this leads to enhancement of photocatalytic activity.

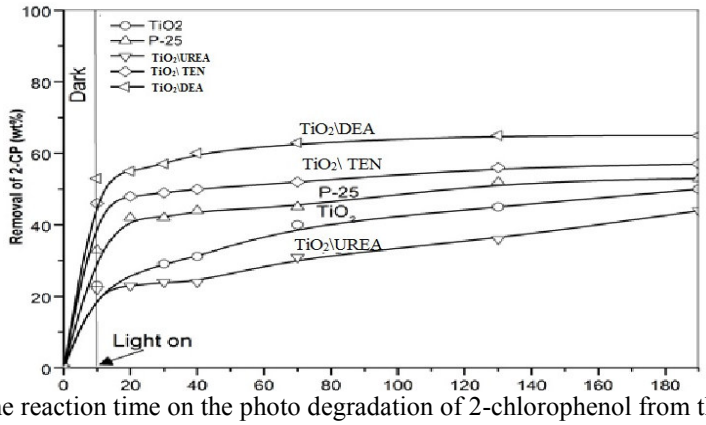

Figure 7. The effect of the reaction time on the photo degradation of 2-chlorophenol from the polluted water.

In heterogeneous photo catalysis, the illumination of semiconductor produces electrons (e-) and holes (h+). The holes (h+) are combining with OH ions and there is formation of hydroxyl radical

(h+vb + OH- → .OH). These surface hydroxyl radicals formed on the surface of the photo-catalyst are oxidizing species which ultimately affects the photo-catalytic activity. This suggests that the increase in hydroxyl content of the film increases the photo-catalytic activity. These results indicated that N-doped TiO_2 has catalytic ability in the visible region. The maximum degradation of 2-CP for TiO_2\DEA nanoparticles can be attributed to lowest band gap energy, smaller particles and more hydroxyl concentration on the surface of the oxide surface. In

the present investigations, the TiO_2\DEA nanoparticles have better photocatalytic activity than lower N-doped or p-25 and un doped TiO_2.

Although nitrogen content in doped TiO_2 increase the photocatalytic degradation, On the contrary TiO_2\UREA have less catalytic degradation when compared with TiO_2 or P-25, this result is attributed to the low concentration of nitrogen in TiO_2\UREA, nitrogen ions are not well distributed in TiO_2 Lattice. It is widely accepted that the doped nitrogen ions will change from the trapping centers to recombination centers as the doped in unsuitable concentration.

3.9. *Effect of intermediates products on the photocatalytic activity.*

Catechol (CT) is known to be strongly adsorbed on the catalyst surface [28], forming long wavelength absorbing complexes on the surface of the catalyst. The formation of this complex produces hydronium ion, which control desorption of CT from the surface to the bulk solution [29-30]. However, the strong adsorption of CT on the catalyst surface decreases the photocatalytic degradation of 2-CP. Also, the mineralization of CT could be responsible for the decrease of pH and inhibit the formation of •OH which is necessary to initiate a further degradation.

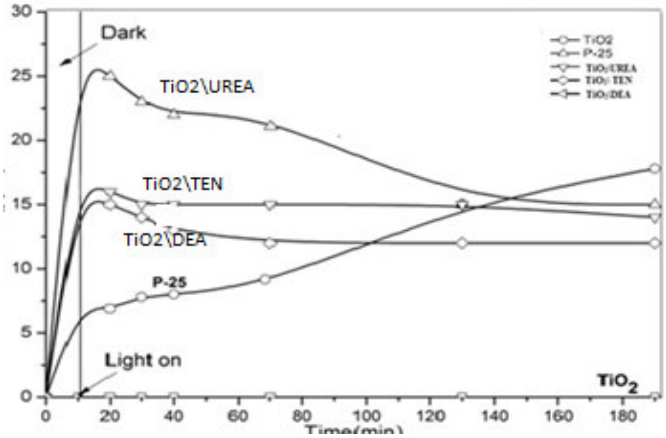

Figure 8. Effect of the reaction time on the production of catechol in the photo degradation of 2-chlorophenol from the polluted water.

Catechol is the only aromatic intermediate identified by HPLC during the degradation process of 2-CP [31]. As shown in Figure 8, CT appeared from the very beginning, it soon reached a maximum concentration of 25, 17, 15 ppm for TiO_2\UREA, TiO_2\TEN and TiO_2\DEA respectively at 20 min. The concentration then very slightly decreases to reach 17, 15 and 12.5 ppm for TiO_2\UREA, TiO_2\TEN and TiO_2\DEA respectively after180 min.

The presence of CT in the aqueous phase compete with 2-CP in the adsorption on the surface of the catalyst and hence decrease the photocatalytic degradation of 2-CP. Figure 8, also shows that, as doping concentration increase, the formation of CT decreases. Since the TiO_2\DEA show the less production of CT after 180 min, this result explains why the high photocatalytic activity of TiO_2\DEA.

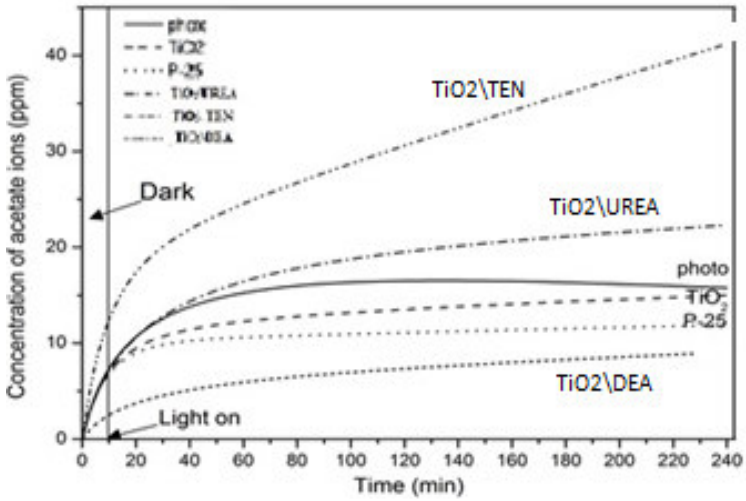

Figure 9. Effect of the reaction time on the production of acetate ions in the photo degradation of 2-chlorophenol from the polluted water.

As shown in Figure 9, the effect of the reaction time on the production of acetate ion, TiO_2\DEA has the lowest of acetate concentration (8 ppm at 240 min) compared with TiO_2\UREA and TiO_2\TEN or pure TiO_2 and P-25,. This means that, the concentration of acetate ion decrease with increasing the concentration of nitrogen doping.

The higher acetate ions concentration decreases the pH value of the aqueous solution. The decrease in pH showed a decrease in the photo-degradation efficiency. Since the protons are potential determining ions for TiO_2, the surface charge development is affected by the pH [32]. Upon hydration, surface hydroxyl groups (TiOH) are formed on TiO_2. These surface hydroxyl group scan undergo proton association or dissociation reactions, thereby bringing about surface charge which is pH-dependent:

$$TiOH + H^+ \rightleftharpoons TiOH_2^+$$

$$TiOH \rightleftharpoons TiO^- + H^+$$

Where TiOH2+, TiOH, and TiO− are positive, neutral and negative surface hydroxyl groups, respectively. A low pH is associated with a positively charged surface which cannot provide hydroxyl groups which are needed for hydroxyl radical formation. Consequently, the rate of 2-CP degradation decreases. On the other hand, higher pH value can provide higher concentration of hydroxyl ions (OH−) to react with the holes to form hydroxyl radicals (OH•), thereby TiO2\DEA enhancing the photo-degradation of 2-CP [33].

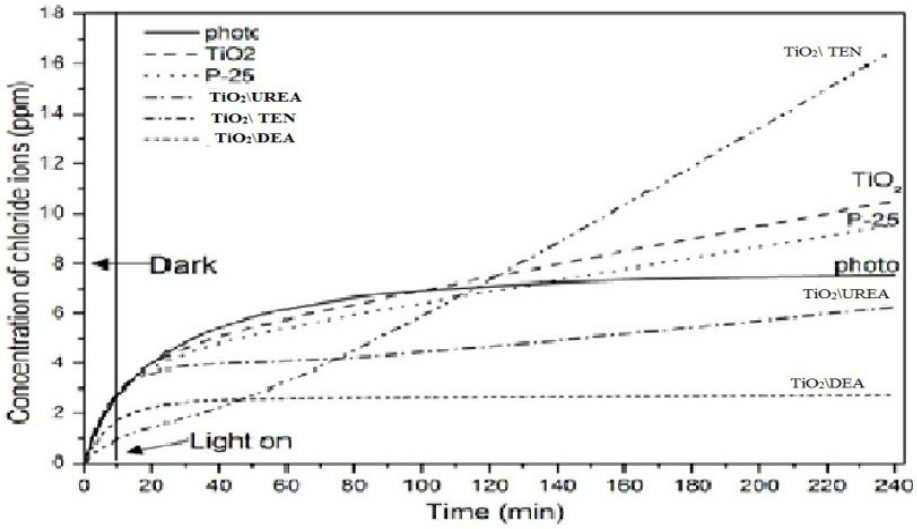

Figure 10. Effect of the reaction time on the production of Chloride ions in the photo-degradation of 2-chlorophenol from the polluted water.

As shown in Figure 10, the effect of the reaction time on the production of chloride ions , TiO_2\DEA has the lowest of chloride concentration (2.5 ppm after 240 min) compared with TiO_2\UREA and TiO_2\TEN or pure TiO_2 and P-25,. This means that, the concentration of chloride ions decrease with increasing the concentration of nitrogen doping. The higher chloride ions concentration acts as hydroxyl radical scavenger. Chloride ions can also absorb UV light and therefore TiO_2\DEA enhancing the photo-degradation of 2-CP.

Conclusion

Different nitrogen dopants display difference in visible light absorption abilities, band gap energies of the N-doped TiO_2 and consequently, photocatalytic efficiencies of TiO_2 during the photo-degradation of 2-CP. Amongst three nitrogen dopants, DEA provided the interstitial N-doped TiO_2 the interstitial N-doped TiO_2 with highest visible light absorption ability and highest efficiency in 2-CP degradation. The photocatalytic activity and 2-CP mineralization ability of all N-doped TiO_2 can be arranged in the following order: TiO_2/DEA > TiO_2/TEN > TiO_2/UREA > un-doped TiO_2.

References

1. Fujishima, A. & Honda, K. (1972), “Electrochemical photolysis of water at a semiconductor electrode”, Nature, 238, 37—38.
2. Gole, J.L.; Stout, J.D.; Burda, C.; Lou, Y. & Chen, X. (2004),“Highly efficient formation of visible light tunable TiO2-xNx photocatalysts and their transformation at the nanoscale”, J. Phys. Chem. B, 108(4), 1230—1240.

3. Wang, Z.; Cai, W.; Hong, X.; Zhao, X.; Xu, F. & Cai, C. (2005), "Photocatalytic degradation of phenol in aqueous nitrogen-doped TiO2 suspensions with various light sources", App. Catal. B, 57(3), 223—231.
4. Nakamura, R.; Tanaka, T. & Nakato, Y. (2004), "Mechanism for visible light responses in anodic photocurrents at N-doped TiO2 film electrodes", J. Phys. Chem. B, 108(30), 10617—10620.
5. Jang, J.S.; Kim, H.G.; Ji, S.M.; Bae, S.W.; Jung, J.H.; Shon, B.H. & Lee, J.S.(2006), "Formation of crystalline TiO2-xNx and its photocatalytic activity", J. Solid State Chem., 179(4), 1067—1075.
6. Yin, S.; Ihara, K.;, Komatsu, M..; Zhang, Q.; Saito, F.; Kyotani, T. & Sato, T. (2006), "Low temperature synthesis of TiO2-xNy powders and films with visible light responsive photocatalytic activity", Solid State Commun., 137(3), 132—137.
7. Kieth, L.H. (1980), " EPA's priority pollutants: where they come from where they're going? " AIChE Symp. Ser., Water 77(209), 249.
8. Irie, H.; Watanabe, Y..& Hashimoto, K. (2003), "Nitrogen-concentration dependence on photocatalytic activity of TiO2-xNx powders. J Phys Chem B"; 5483-5486.
9. Juan, K.D. (1984), "The fundamental and practice for the removal of phenolic compounds in wastewater", Industrial Pollut. Prevention Control 3(3), 88.
10. Shibaeva, I.V., Metelitsa, D.I. & Denison, E.T. (1969), "The oxidation of phenol with molecular oxygen in aqueous solution II. The role of hydrogen in the oxidation of phenol with oxygen" , Kinet. Catal. (10), 1022.
11. Eisenhauer, H.R. (1968), "The ozonization of phenolic wastes", J. Water Pollut. Control Fed. 40(11), 1887.
12. Moza, D.N., Fytianos, K., Samanidou, V. & Korte,F.(1988), "Photodecomposition of chlorophenols in aqueous medium in pressence of hydrogen peroxide", Bull. Environ. Contam. Toxicol. (41), 678.
13. Haggblom, M. (1988), "Degradation and transformation of chlorinated phenolic compounds by strain of Rhodococcus and Mycobaterium", Water Res. 22(2) 171
14. Dorn, E. (1988), "Isolation and characterization of a 3-chlorobenzoate degrading Psudomonas, Arch. Microbiol". 99, 61.
15. Shen, Y.S. & Ku, Y. (1995), "The study and application of advanced oxidation processes in volatile organic compounds", Industrial Pollut. Prevention Control 56, 278.
16. Ollis, D.F.; Pelizzetti, E., & Sperone, N. (1989), "Heterogeneous photocatalysis in the environment: application to water purification, in: N. Sperone, E. Pelizzetti (Eds.) ", Photocatalysis Fundamentals and Applications Wiley, Chichester, , p. 603.
17. Cullity, B.D. (1978), "Elements of X-Ray Diffraction", 2nd Ed, Addison- Wesley, MA, USA, 102 Irie, H.; Watanabe, Y..& Hashimoto, K. (2003), "Nitrogen-concentration dependence on photocatalytic activity of TiO2-xNx powders. J Phys Chem B"; 5483-5486.
18. Ihara, T.; Miyoshi, M.; Triyama, Y.; Marsumato, O. & Sugihara, S. (2003) "Visible-light-active titanium oxide photocatalyst realized by an oxygen-deficient structure and by nitrogen doping". Appl Catal B 42, 403-409.
19. Zhao, Z, Liu, Q. (2008) "Mechanism of higher photocatalytic activity of anatase TiO2 doped with nitrogen under visible-light irradiation from density functional theory calculation". J Phys D Appl Phys 41: 1-10.
20. Sato, S. (1986) "Photocatalytic activity of NOx-doped TiO2 in the visible light region". Chem Phys Lett 123, 126-128.
21. Vijayalakshmi, R.; & Rajendran, V.; (2012),"Synthesis and characterization of nano-TiO_2 via different methods" Archives of Applied Science Research, 2, 1183-1190.
22. Balachandran U; &N.G. Eror (1982) "Raman spectra of titanium dioxide" Journal of Solid State Chemistry 42, 276- 282.
23. Liu, Y.; Chen, X.; Li, J. & Burda, C. (2005), Photocatalytic degradation of azo dyes by nitrogen-doped TiO2 nanocatalysts. Chemosphere. 61:11-18.
24. Puma G.L; & Yue, P.L. (2002) "Effect of radiation wavelength on the rate of photocatalytic oxidation of organic pollutants" Industrial and Engineering Chemistry Research, 41, 5594- 5600.
25. Tsai, S. & Cheng, S. (1997) "Effect of TiO_2 crystalline structure in photocatalytic degradation on of phenolic contaminants" Catalysis Today, 33, 227-237.
26. Chen F.; Zhao, J. & Hidaka, H. (2003) "Adsorption factor and photocatalytic degradation of dye-constituent aromatics on the surface of TiO_2 in the presence of phosphate anion" Research on Chemical Intermediates 29, 733-748.
27. Hsien, V.H,; Chang, C. F.; Chen, Y.H.; & S.Cheng (2001) "Photodegradation of aromatic pollutants in water over TiO_2 supported on molecular sieves". Applied Catalysis B: Environmental, 31, 241-245.
28. Abdel-Aal, A.A..; Mahmoud, S.A. & Aboul-Gheit, A.K. (2009), "Sol–Gel and Thermally Evaporated Nanostructured Thin ZnO Films for Photocatalytic Degradation of Trichlorophenol" Nanoscale Research Letters, 4, 627-634.
29. Cho, Y.M.; Choi, W.Y.; Lee, C.H.; Hyeon, T.H. & Lee, H.I. (2001) "Visible light-induced degradation of carbon tetrachloride on dye-sensitized TiO_2" Environmental Science & Technology, 35, 966-970.

30. Xu, N.; Shi, Z.; Fan, Y.; Shi, J. & Hu, M.Z.C. (1999) "Effects of particle size of TiO_2 on photocatalytic degradation of methylene blue in aqueous suspensions" Industrial and Engineering Chemistry, 38, 373-379.
31. Ilisz, I.; Dombi, A.; Mogyorosi, K.; Farkas, A. & Dekany, I. (2002), "Removal of 2-chlorphenol from water by adsorption combined with TiO_2 photocatalysis" Applied Catalysis B: Environmental, 39, 247-256.
32. Jankovic I.A., Dzunuzovic, E.S. & Nedeljkovic, J.M. (2010) "New Hybrid Properties of TiO_2 Nanoparticles Surface Modified With Catecholate Type Ligands "Nanoscale Research Letters, 5, 81-88.
33. Betiha M. A.; Mahmoud; S. A., . Menoufy, M. F. & Al-Sabagh, A. M. (2011), "One-pot template synthesis of Ti–Al containing mesoporoussilicas and their application as potential photocatalytic degradation of chlorophenols" Applied Catalysis B: Environmental, 107, 316– 326.